Materials Today Communications 33 (2022) 104512

Contents lists available at ScienceDirect

Materials Today Communications

journal homepage: www.elsevier.com/locate/mtcomm

Microstructure and mechanical properties of aluminum matrix composites with bimodal-sized hybrid NbC-B_4C reinforcements

Aicha S. Lemine [a,b], Osama Fayyaz [c], Moinuddin Yusuf [c], R.A. Shakoor [a,c,*], Zubair Ahmad [b,c], Jolly Bhadra [b,c], Noora J. Al-Thani [b]

[a] Department of Mechanical and Industrial Engineering, College of Engineering, Qatar University, 2713 Doha, Qatar
[b] Qatar University Young Scientists Center (QUYSC), Qatar University, 2713 Doha, Qatar
[c] Center for Advanced Materials (CAM), Qatar University, 2713 Doha, Qatar

ARTICLE INFO

Keywords:
Aluminum
Hybrid composites
Mechanical properties
Mechanical milling
Microwave sintering

ABSTRACT

Aluminum (Al) is an earth-abundant metal recognized with superior properties for vital applications in the aerospace and transportation industries. Structural components of Al exhibit poor performance due to its inherent low mechanical strength. In this work, the mechanical properties of Al are enhanced by reinforcing with bimodal micron-sized Niobium Carbide (NbC) and nano-sized Boron Carbide (B_4C) ceramic particles. Al-NbC-B_4C hybrid composites have been synthesized via ball milling followed by cold compaction and microwave sintering. NbC micro-reinforcement composition has been kept fixed (5 wt%), while B_4C nano-reinforcement composition varied from 0.5 wt%, 1.0 wt%, 1.5 wt%, and 2.0 wt%. XRD patterns revealed the high crystallinity with no detected new phases formed in the sintered composites. TEM micrographs presented the microstructure evolutions with uniform distribution of (micron + nano) hybrid bimodal-sized ceramic reinforcements in the Al matrix. FE-SEM micrographs and corresponding elemental mapping demonstrated the homogeneity in the elemental distribution of synthesized Al-NbC-B_4C composites through the ball milling and microwave sintering processes. Roughness values and AFM images showed the formation of insoluble secondary phases dispersed in the Al matrix enhancing its surface resistance towards localized plastic deformations. Al-5 wt%NbC-2.0 wt%B_4C composite has exhibited an ultrahigh improvement in the mechanical properties compared to pure Al. It showed enhancements in microhardness (46%), nanohardness (54%), and Young's modulus (31%). It also showed high ultimate compression strength of 328 MPa and a low engineering failure strain of 0.64. FE-SEM compressive fractography confirmed the strengthened dispersion hardening effect from bimodal-sized ceramic particles obstacle multi-length cracks and resisting fracture failure.

1. Introduction

Aluminum (Al) and its alloys provide the end-user with lightweight components of high commercial demand for electronic, aerospace, and automobile applications but exhibit poor performance due to its low mechanical strength [1,2]. Mostly, the mechanical properties of Al and its alloys could be enhanced via synthesizing mono-modal (micron or nano), bimodal (micron + nano), or hybrid ceramic particles reinforced Al matrix composites (AMCs) [3]. In literature, the hybrid AMCs have been categorized based on the type of particulate reinforcement into an industrial-waste derivative with synthetic ceramic material, an agro-waste derivative with synthetic ceramic material, and two synthetic ceramic materials [3]. AMCs have been reinforced with Al_2O_3/B_4C [4], SiC/TiB_2 [5], TiC/CNT [6], and micro/nano Al_2O_3 [7] to improve their tribological, corrosion, and mechanical properties.

Nano-sized particle reinforcements play a crucial role in enhancing the mechanical properties of AMCs through dispersion strengthening with a significant decline in ductility [8]. Difficulties in dispersion and reinforcement agglomeration in the matrix have led to minimizing the effective volume fraction of nano-reinforcement to be kept around 2% [9]. Whereas, the micron-sized particle reinforcement could achieve higher volume fractions as 40% [9]. The effective weight composition of micron-sized reinforcements in Al matrix composites is 5 wt%, as frequently reported in the literature [10–12]. For instance, the addition of micron-sized reinforcement into the Al matrix such as Alumina (Al_2O_3) has resulted in a high agglomeration and low segregation of

* Corresponding author at: Department of Mechanical and Industrial Engineering, College of Engineering, Qatar University, 2713 Doha, Qatar.
E-mail address: shakoor@qu.edu.qa (R.A. Shakoor).

https://doi.org/10.1016/j.mtcomm.2022.104512
Received 23 July 2022; Received in revised form 5 September 2022; Accepted 19 September 2022
Available online 21 September 2022

micron particles, particularly at compositions higher than 5 wt% [13]. However, the discontinuity in the matrix material might be raised with the large size of the reinforcement, causing the deterioration of composite ductility [10]. The bimodal-sized reinforced composites with a mixture of nano- and micron-sized (bimodal-sized) particles advantage of a high-volume fraction without intense ductility reduction [10]. Recently, it is extensively reported enhancements in the mechanical properties of AMCs in conjugate to reinforcing bimodal-sized particles [14,15].

The wear and tensile properties of hybrid Al-5 wt%SiC-2 wt%CNTs composite have overcome mono-reinforced composites of only SiC or CNTs [16]. This improvement in mechanical properties is referred to as the synergistic effect of strengthening mechanisms caused by different reinforcements length-scale (micron+nano) [16]. Another study has enhanced the yield and ultimate strengths of the Al matrix by 23% and 64%, respectively via the addition of equivalent composition of 10 wt% nano-sized TiB_2 and micro-sized SiC reinforcement particles [17]. However, the fractured surface resembled a brittle fracture because of the large size around 13 μm of micro-SiC reinforcement. It is reported that the properties of micron-sized reinforced composites decay with increasing the size of reinforcement particles [18]. Consequently, the mechanical properties of hybrid AMCs are influenced not only by the fabrication route but by a combination of multiple factors.

Niobium Carbide (NbC) ceramic particles own high hardness (2400HV), high elastic modulus (338.5 GPa), high melting point (3490 °C), low linear expansion coefficient (6.5 $\times 10^{-6}$ K^{-1}), high physical and chemical stabilities [19,20]. The NbC has a crystal structure of Face Centered Cubic (FCC) with lattice parameters of a=b=c= 0.447 nm [19]. It has orientation relationships with α-Al as $\{111\}_{Al}$ || $\{200\}_{NbC}$ and $< 112 >_{Al}$ || $< 100 >_{NbC}$, which could form semicoherent or coherent interfaces with α-Al matrix [20]. The formation of such interfaces between the matrix and reinforcement phases is advantageous for improving the interfacial bonding strength and reducing the interface energy [20].

Boron Carbide (B_4C) is also an attractive reinforcement ceramic particle in the Al matrix due to its ability to absorb neutrons, low thermal expansion coefficient (5 $\times 10^{-6}$ K^{-1}), high thermal conductivity (29 W/m.K), excellent chemical and thermal stabilities, high elastic modulus (460 GPa), high compressive strength (3000 MPa), and excellent wear resistance [21,22]. It has a higher hardness (9.35 by Mohs Hardness Scale) and lower density (2.52 g/cm^3) compared to SiC and Al_2O_3 [21]. It is suitable for use in bulletproof vests, bicycle frames, armor tanks, and neutron shielding applications [22]. The Al/B_4C composites have been reported frequently with better interfacial bonding and superior particle distribution in comparison to Al/SiC and Al/Al_2O_3 composites [23,24]. The B_4C preserves its hardness at elevated temperatures, which enables its use in high-temperature applications reaching 2000 °C [23].

The crucial challenges in the fabrication of AMCs are the defect-free microstructure, wettability of reinforcement with matrix, and homogenous reinforcement distribution [24]. There are commonly reported fabrication methods of AMC classified into liquid-state processing as stir, squeeze, or spray casting and solid-state processing as mechanical alloying, powder metallurgy, and sintering [25,26]. The production route of AMC via powder metallurgy (PM) is an effective technique for synthesizing micro- and nano-ceramic reinforced particles [25]. It is an alternative production route to conventional casting processes for homogenous distribution of dispersed phases in the matrix, adequate interfacial bonding among the matrix and reinforced phases, and preventing the formation of undesirable phases [26]. PM has emerged as the most common and easy fabrication technique applicable to most materials and produces good quality composites [26].

The original value of this paper is to investigate the in-situ hybrid compositing of Al matrix with ceramic reinforcement particles of NbC and B_4C. Through systematic research, this present work will use reinforcements in bimodal particle size distribution to examine their synergistic effect on the mechanical behavior and microstructure of the resultant Al/micro-NbC/nano-B_4C hybrid composite. The fabrication route adopted in this study is based on facile, cost-effective, and good-quality synthesis processes namely, mechanical milling and microwave sintering processes, as illustrated in Fig. 1. The Al-NbC-B_4C composites will be synthesized in three stages starting with mechanical milling to blend homogeneously at the solid-state matrix and reinforcement powders in a ball milling process. The resultant milled composite powder will then undergo consolidation into cylindrical pellets using cold compaction, as demonstrated in Fig. 1. The composite pellets will go through fast, uniform, and high-degree densification via a non-conventional microwave sintering technique using electromagnetic radiation to enhance their microstructure and mechanical properties.

2. Experimental

2.1. Samples preparation and processing methods

The high purity elemental powder of Al (99.5%, 7–15 μm, Alfa Aesar) was used as the matrix material for Al-NbC-B_4C hybrid composites. The reinforcement materials were the high purity NbC powder (99.9%, 1–3 μm, US Research Nanomaterials Inc.) and B_4C nanopowder (99%, 45–55 nm, US Research Nanomaterials Inc.). The powders were weighed in certain compositions with a fixed 5.0 wt% of NbC micropowder and different weight fractions of 0.5 wt%, 1.0 wt%, 1.5 wt%, and 2.0 wt% B_4C nano-powder, as displayed in Table 1.

The weighted powders were then loaded into stainless steel (SS) vial with a 1:1 ball-to-powder ratio (BPR) and milled using a planetary ball milling device (PM200, RETSCH 20.640.0001, Haan, Germany) for 2 h at a rotation speed of 200 rpm. The milled powder of 1 g was cold compacted under a uniaxial pressure of 50 MPa for 1 min in a cylindrical SS die with a diameter of 12.92 mm. The cylindrical pellets were then sintered through a bidirectional microwave-assisted rapid sintering technique (VB ceramic furnace, VBCC/MF/1600 °C/14/15, Chennai, India) at a uniform temperature of 550 °C, constant heating/cooling rate of 10 °C/min, and dwell time of 30 min. The sintered pellets were cooled down to room temperature of 25 °C before their polishing and then characterization via different techniques.

2.2. Characterization Techniques

2.2.1. Structural and Morphology

The X-ray diffraction (XRD: PANalytical, EMPYREAN) was used for the phase identification of the polished sintered samples using Cu/Kα radiation source and a wavelength of 1.54 Å. The microstructure features of the synthesized samples were investigated via Transmission electron microscopy (TEM: Tecnai G2 FEG 200 kV, FEI) on milled powders and Field emission scanning electron microscopy (FE-SEM: Nova NanoSEM 450, FEI) in conjugation with Energy dispersive X-ray spectroscopy (EDX) on both polished pellets and compression fractured pellets. The surface topography of polished pellets was studied using Atomic force microscopy (AFM: MFP 3D-Asylum Research). The density and porosity measurements were carried on the sintered pellets based on Archimedes' principle (Density kit analytical balance, YDK03, sartorius).

2.2.2. Mechanical properties measurements

The microhardness of polished pellets was measured using a Vickers microhardness tester (FM-ARS9000, Future-Tech) with a 4-sided pyramid tip at a test load of 50gf for 10 s and 5 successive iterations per sample. The nanohardness was carried on the polished pellets using a nanoindenter (MFP-3D NanoIndenter, Asylum Research) with a 3-sided pyramid tip at a maximum load of 1mN and dwell time of 5 s at the peak load. The compression strength and Young's modulus were measured on the pellets using a universal testing machine (LR 50 K Plus – Lloyd Instruments) based on ASTM E9–89a and at a constant engineering strain

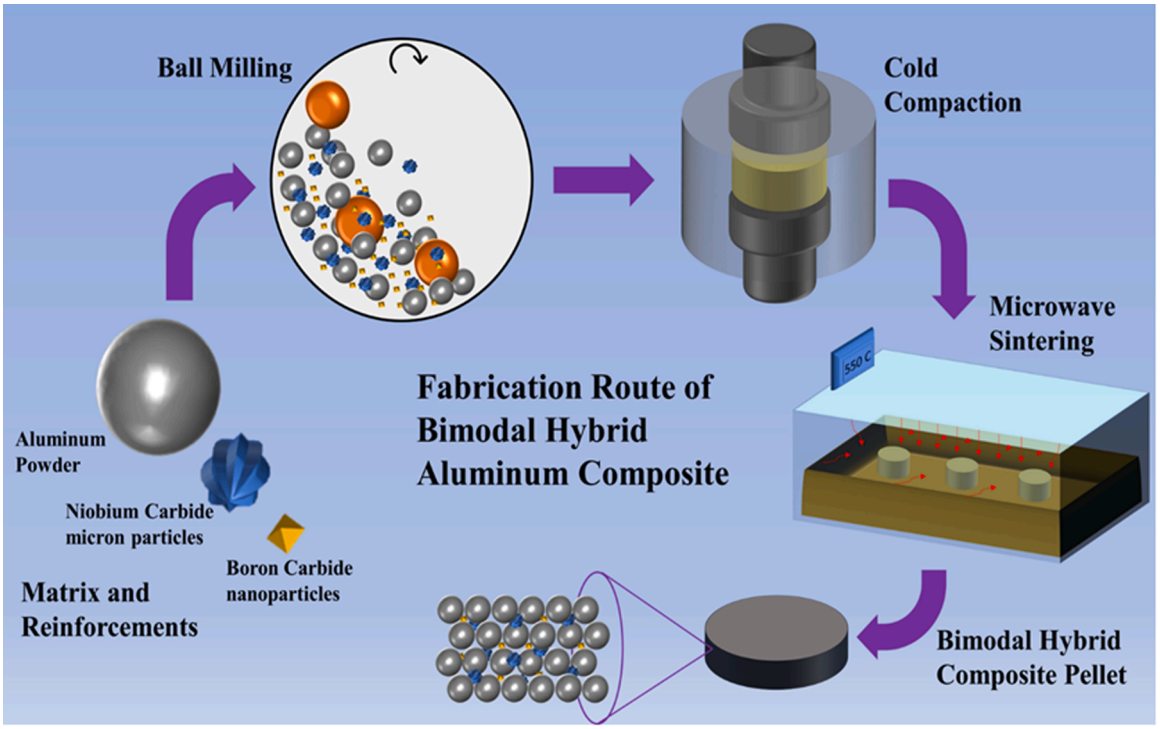

Fig. 1. Schematic illustration of preparation and processing methods for Al-NbC-B_4C samples.

Table 1
Weight compositions of prepared samples.

Sample Code		NbC amount (wt%)	B_4C amount (wt%)	Al amount (wt %)
S1	Pure Al	0	0	100
S2	Al-5 wt% NbC	5.0	0	95
S3	Al-5 wt% NbC-0.5 wt% B_4C	5.0	0.5	94.5
S4	Al-5 wt% NbC-1.0 wt% B_4C	5.0	1.0	94
S5	Al-5 wt% NbC-1.5 wt% B_4C	5.0	1.5	93.5
S6	Al-5 wt% NbC-2.0 wt% B_4C	5.0	2.0	93

rate of 0.6 mm/min. These mechanical measurements were conducted at room temperature and repeated five times for each sample.

3. Results and discussions

3.1. Structural and morphology

3.1.1. XRD analysis of Al-NbC-B_4C hybrid composites

The crystallographic structure of the microwave sintered pellets of pure Al and Al-NbC-B_4C composites are well consistent with sharp and narrow peaks, as shown in Fig. 2. Bragg's fundamental peak for the Al and its composites appears with an indexed crystal plane of (111) at a low Bragg's angle (2θ) of 38.5° in very strong intensity. The characteristic peaks of XRD patterns are consistent with the standard peaks of FCC Al metal in the Inorganic Crystal Structure Database (ICSD-166867) [27]. The good agreement in the peak intensities and positions points to the uniform crystallographic structure of synthesized Al-NbC-B_4C composites with defect-free microstructure. The NbC micro-reinforcement shows diffraction peaks at 2θ of 22.6°, 28.4°, and 43.2° corresponding to low-intensity peaks indexed with planes of (010), (111), and (112), respectively. These XRD peaks are consistent with the standard peaks of FCC NbC metal in the ICSD-44355 [28].

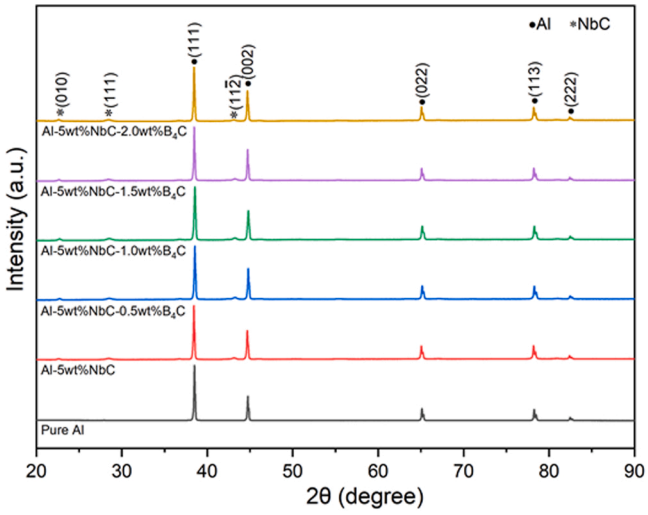

Fig. 2. XRD patterns for pure Al and Al-NbC-B_4C hybrid composites.

The diffraction peaks of B_4C nano-reinforcement have not been detected in the diffraction patterns of synthesized Al-NbC-B_4C composites, which are ascribed to the small composition of the added B_4C (≤2.0 wt%). The low contents of B_4C nano-reinforcement might facilitate the uniform dispersion in the Al matrix to strengthen its dispersion hardening effect [9]. Additionally, the XRD patterns show the absence of any extra peaks indicating impurities or undesired phases formed in the Al composites, particularly the aluminum oxide (Al_2O_3) and carbide (Al_4C_3) phases. The formation of the Al_4C_3 phase has been observed commonly for composites fabricated from powder mixture undergoing excessive ball milling exceeding 4hrs [29] or sintering temperatures above 600 °C [30]. This will simulate the interfacial reactions between the Al matrix and C atoms diffused from defective regions of NbC and B_4C [31]. However, the adopted experimental conditions in milling (2hrs) and sintering (550 °C) of Al-NbC-B_4C samples were adequate to

evade the formation of the Al_4C_3 phase and sustain the crystalline character of Al composites.

Additionally, the broadening in the observed XRD peaks profile of synthesized samples gives a reliable insight into their average crystallites size, which has been quantified using the Warren-Averbach method [32]:

$$\frac{\beta_{hkl}{}^2}{\tan^2\theta} = \frac{\lambda}{D}\left(\frac{\beta_{hkl}}{\tan\theta\sin\theta}\right) + 25 \quad \langle\varepsilon^2\rangle \tag{1}$$

Where D is the average grains size, ε is the microscopic lattice strain, θ is the diffraction angle of the peak in radian, λ is the wavelength of the x-rays beam, and β_{hkl} is the FWHM of the peak (hkl) in radian [32]. The calculations of average grain size are based on the highest intensity peaks: (111), (002), (022), (113), and (222). Fitting the data of $\beta^2_{hkl}/\tan^2\theta$ vs $\beta_{hkl}/(\tan\theta.\sin\theta)$ through Gaussian function gave the best-fitting linear regression model to all of the recognized diffraction peaks in XRD patterns of either pure Al or Al-NbC-B_4C composites. This resulted in high R^2 values of their linear trend lines being always close to 1, which verifies the reported average grain size of synthesized samples. The synthesized pure Al shows an average grain size of 54 nm, as displayed in Table 2. Whereas, the average grain size for the microwave sintered Al-NbC-B_4C composites was found to be around 17 nm and then was considerably affected by the addition of bimodal-sized hybrid NbC-B_4C reinforcements during the mechanical milling process, as shown in Table 2. These ultrafine grains of Al-NbC-B_4C composites might contribute to enhancements of their mechanical properties based on the Hall-Petch effect compared to coarse-grained pure Al [33]. The Hall-Petch effect states that the increase in the hardness of a material is associated with a reduction in its average grain size [34,35].

3.1.2. TEM analysis of Al-NbC-B_4C hybrid composites

The TEM analysis was carried out on the Al composites to investigate their microstructure evolutions. Fig. 3(a and b) show the microstructure features of hybrid composites based on an Al matrix reinforced with micro-NbC and nano-B_4C hard ceramic particles. The bright-field (BF) TEM images represent the even and uniform dispersion of bimodal-sized hybrid NbC-B_4C reinforcements in the Al matrix without noticing agglomerated crystallites. The homogeneous dispersion of reinforcement particles in the Al matrix was attainable through the planetary ball milling process for 2 h and 1:1 BPR. This will enhance the interfacial strength of the Al composites, hence increasing their load transfer. Fig. 3c shows the Selected Area Diffraction Pattern (SADP) on the detected grains in the BF TEM image of the Al-5 wt%NbC-1.0 wt%B_4C composite. The grains in SADP appear to be equiaxed in circular rings and random orientations, hence matching their diffraction profile in the XRD pattern.

The High-resolution TEM images in Fig. 3(d and e) show visible interfaces between the Al matrix and NbC-B_4C reinforcements. The interplanar spacing of the Al matrix and B_4C nano-reinforcement has been observed in the HR TEM images, as displayed in Fig. 3(d and e). The interplanar spacing of the Al matrix is 0.116 nm corresponding to the XRD diffraction plane of (222), which is observable in the Al-5 wt% NbC composite. The HR TEM image of Al-5 wt%NbC-1.0 wt%B_4C showed the interplanar spacing of B_4C reinforcements at different areas as 0.152 nm, 0.318 nm, and 0.343 nm corresponding to the XRD diffraction planes of (044$^-$), (200), and (011), respectively. Fig. 3f shows the HR TEM image on a 5 nm scale for Al-5 wt%NbC-1.0 wt%B_4C composite with noticeable long-range atomic arrangements in defect-free microstructure matching the high crystallinity character as pre-observed from the sharp and narrow XRD diffraction patterns.

Table 2
Integral breadth analysis on the XRD patterns of Al-NbC-B_4C hybrid composites using the Warren-Averbach method.

Sample		Grain size (nm)	Lattice strain (%)
S1	Pure Al	54	0.06
S2	Al-5 wt% NbC	13	0.23
S3	Al-5 wt% NbC-0.5 wt% B_4C	18	0.17
S4	Al-5 wt% NbC-1.0 wt% B_4C	17	0.19
S5	Al-5 wt% NbC-1.5 wt% B_4C	17	0.18
S6	Al-5 wt% NbC-2.0 wt% B_4C	17	0.18

3.1.3. FE-SEM elemental mapping analysis of Al-NbC-B_4C hybrid composites

The elemental mapping obtained by FE-SEM through EDX was used to investigate the homogeneity and distribution of Al-NbC-B_4C composite constituents. Fig. 4 shows the FE-SEM micrographs with the corresponding elemental mapping of Al-NbC-B_4C composites containing 0.5, 1.0, and 1.5 wt% B_4C nano-reinforcement. The elemental mapping in Fig. 4 reveals the microstructure of Al hybrid composites with a uniform dispersion of NbC micro-reinforcement added at a fixed composition of 5.0 wt% into the Al matrix, which is consistent with TEM analysis. The non-detecting of the Boron (B) element in the elemental mapping of synthesized Al-NbC-B_4C composites could be ascribed to the small composition of the added B_4C ($\leq$2.0 wt%). The elemental mapping of the Carbon (C) element in Fig. 4 is observed with a homogenous distribution throughout Al-NbC-B_4C composites at different weight compositions of B_4C nano-reinforcement. The homogeneity in the elemental distribution of the C element might point out the uniform distribution of carbon-based ceramic reinforcements (NbC and B_4C) within the Al matrix for Al-NbC-B_4C composites [14,36].

3.1.4. AFM analysis of Al-NbC-B_4C hybrid composites

The AFM analysis was conducted on the sintered pellets to examine the 2D and 3D surface topography along with the roughness-mean-square (RMS) values, as displayed in Fig. 5. The pure Al pellet reveals a very smooth surface with the lowest roughness of 9 nm. The addition of bimodal-sized hybrid NbC-B_4C reinforcements in the Al matrix has increased dramatically the RMS values from 28 nm, 53 nm, to 56 nm for the Al-5 wt%NbC, Al-5 wt%NbC-1.5 wt% B_4C, and Al-5 wt% NbC-2.0 wt%B_4C composites, respectively. A similar trend of RMS incrementations was noticed in relevant previous studies [10,37]. The RMS values trend indicates the formation of secondary phases based on hard and insoluble ceramic micro and nanoparticles, which have been well dispersed during the milling process into the soft Al matrix. This will strengthen the interfaces between the reinforcements and matrix in the composite structure to enhance its mechanical properties. It is worth noting that the Al composites with bimodal (micro+nano) NbC-B_4C reinforcements exhibit more roughness with nearly double RMS values compared to the mono-modal micro-sized NbC reinforcement.

3.1.5. Density and porosity analysis of Al-NbC-B_4C hybrid composites

Archimedes' principle was used for the density and porosity measurements on the sintered Al pellets. Fig. 6 indicates the formation of lightweight Al hybrid composites with increasing the composition of ceramic reinforcement particles. The decrease in the Al matrix density with increasing the B_4C content is due to its replacement with lower-density B_4C nanoparticles. In reverse, the increase in the reinforced hard and insoluble B_4C nanoparticles has increased the porosity of Al composites. The high surface energy of reinforced ceramic nanoparticles might attribute to the formation of insoluble clusters and pore nucleation at the nano-reinforcements surface, particularly at high compositions [38]. Such a trend is consistent with the previously reported studies in the literature for Al hybrid composites with B_4C nanoparticle reinforcements [22]. However, the porosity levels of Al composites have been kept to a minimum by optimizing their synthesis parameters during the milling and sintering processes. The presence of micro-NbC reinforcement particles could also contribute to enhancing the segregation of nano-B_4C reinforcements in the Al matrix.

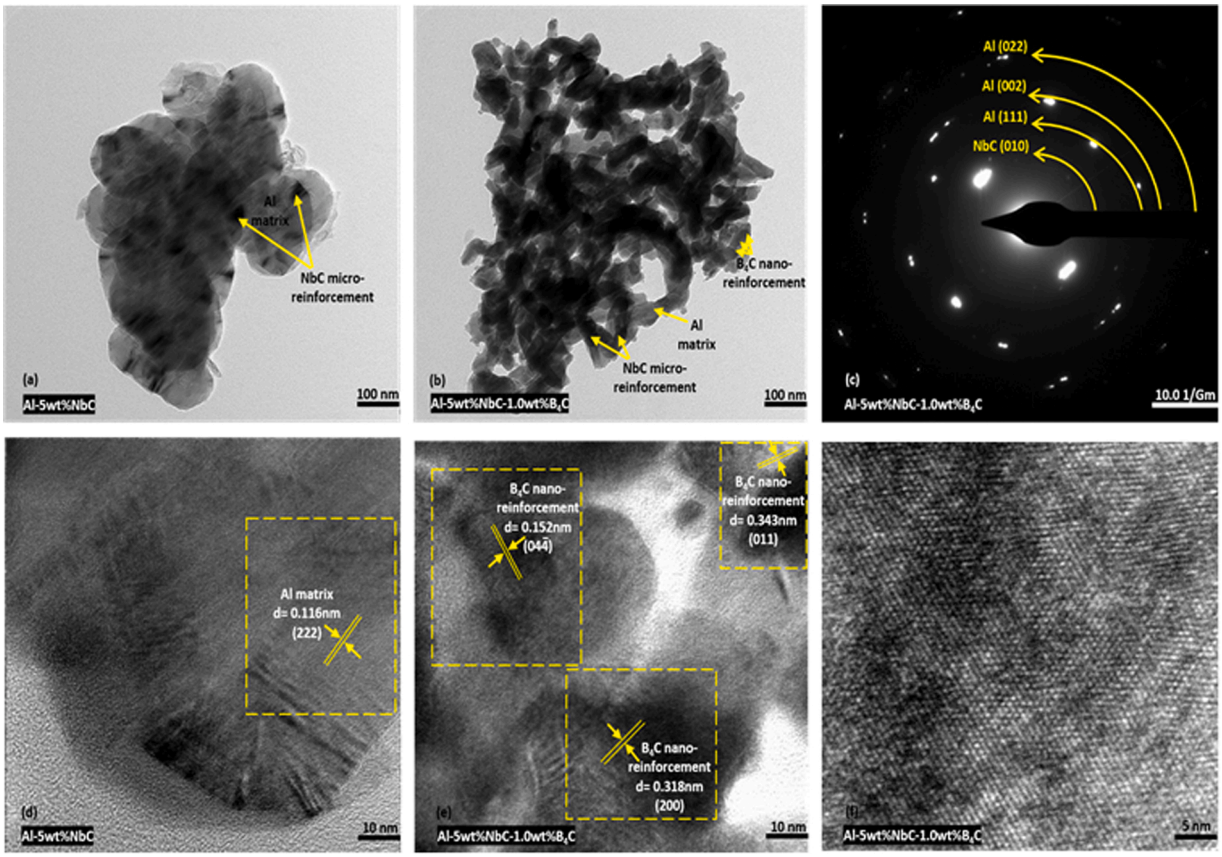

Fig. 3. TEM analysis showing bright-field TEM images of (a) Al-5 wt%NbC composite and (b) Al-5 wt%NbC-1.0 wt%B_4C composite. (c) Diffraction pattern of Al-5 wt%NbC-1.0 wt%B_4C composite. High-resolution TEM images of (d) Al-5 wt%NbC, (e) and (f) Al-5 wt%NbC-1.0 wt%B_4C composites.

3.2. Mechanical properties measurements

3.2.1. Vickers microhardness analysis of Al-NbC-B_4C hybrid composites

The Vickers microhardness measurements were conducted on the polished pellets to examine the surface resistance towards localized plastic deformations using a 4-sided diamond indenter. Fig. 7 displays the gradual incrementation in the Vickers microhardness values with the rise in the composition of hard and nano-sized B_4C reinforcement particles reaching a maximum of 120.4HV. This microhardness has been improved by 46% over pure Al and is comparable to 112HV for Al-15 wt%B_4C mono-reinforced composite prepared via milling followed by microwave sintering and hot extrusion [39]. The bimodal-reinforced Al-5 wt%NbC-2.0 wt%B_4C composite exhibited higher microhardness compared to 66HV and 87HV for the mono-reinforced Al-1.0 wt%Cu composite [40] and bimodal sized reinforced Al-5 wt%Si_3N_4-1.5 wt% GNPs composite, respectively [11]. This is referred to as the enhancements firstly on the load transfer mechanisms via the hybrid compositing of Al with bimodal-sized NbC-B_4C particles. Thus, transferring sufficient load from the soft Al matrix to the hard ceramic reinforcements across the strong matrix-reinforcement interfaces.

Secondly, the improvements in dispersion hardening effect through optimizing the milling process for uniform distribution of hard bimodal-sized NbC-B_4C reinforcements in the Al matrix. The flaky Al particles have a large surface area facilitating the uniform dispersion of both ceramic NbC and B_4C reinforcements with high intrinsic hardness in the Al matrix, as shown in TEM Fig. 3(a and b). This has led to increasing the number of grain boundaries and strengthened matrix-reinforcement interfaces to obstacle the dislocation's motion, hence increasing the hardness values. Thirdly, the grain refinement strengthening of matrix based on the Hall-Petch effect via the reduction in the Al particles size throughout the milling process and insignificant grains growth during the microwave sintering. In conjugate, the grains size of Al composite changes to smaller with increasing replacements of the micro-sized Al particles with nano-reinforced B_4C particles, which is consistent with the integral breadth analysis on their XRD profiles (Table 2). In literature, the nano-sized reinforcements showed a hindering effect on Al grains growth during the sintering [41,42].

3.2.2. Nanohardness analysis of Al-NbC-B_4C hybrid composites

The nanohardness measurements were carried out on the polished pellets using a nanoindenter with a 3-sided pyramid indenter. Fig. 8a shows the load-indentation depth curves of Al-NbC-B_4C composites. The load-indentation curves have shifted toward lower indentation depth with incrementing the composition of hard nano-sized B_4C reinforcements. This has increased the resistance of Al-NbC-B_4C hybrid composites towards the surface deformation caused by nanoindentation load. The nanohardness has been improved by 54% from 1.44 GPa to a maximum of 3.14 GPa for pure Al and Al-5 wt%NbC-2.0 wt%B_4C composite, respectively. This nanohardness value overcomes the 0.899 GPa for Al-5 wt%Si_3N_4-1.5 wt%GNPs composite prepared by a similar route [11] and 0.7 GPa for Al6061-SiC-Graphite hybrid composite synthesized via friction stir process [43]. Fig. 8b shows also the simultaneous decrease in the nanoindentation area from 0.691 μm^2 to a minimum of 0.318 μm^2 for uncomposited Al to Al-5 wt%NbC-2.0 wt%B_4C composited sample. This lower nanoindenter penetration depth indicates the improved surface resistance of Al with micro-NbC and nano-B_4C ceramic particles. This resistance behavior towards localized surface plastic deformations is in agreement with the pre-observed trend in microhardness.

3.2.3. Compression analysis of Al-NbC-B_4C hybrid composites

The ultimate compression strength (UCS) and Young's modulus (E)

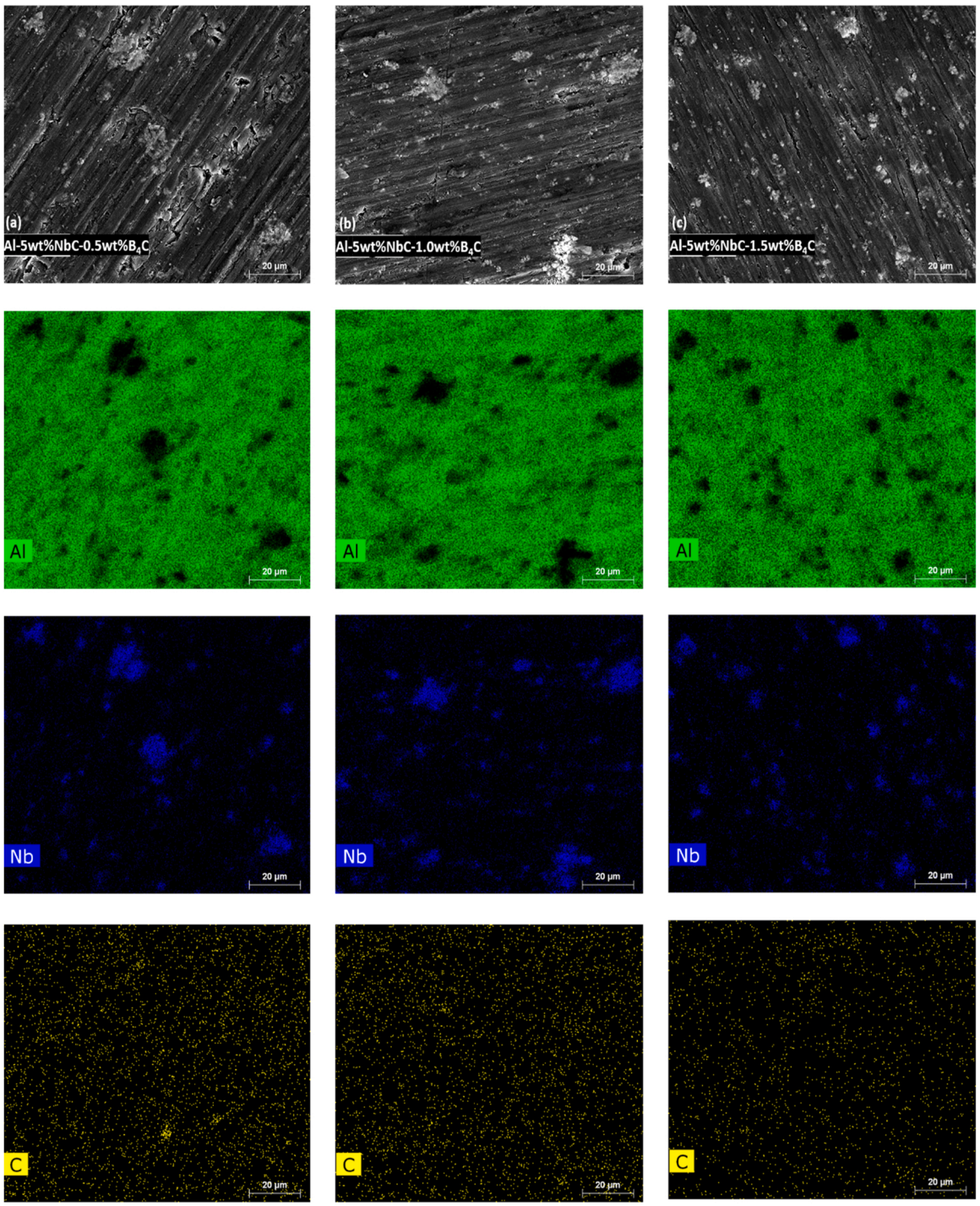

Fig. 4. FE-SEM Microstructure evolutions and corresponding EDX elemental mapping of (a) Al-5 wt%NbC-0.5 wt%B_4C, (b) Al-5 wt%NbC-1.0 wt%B_4C, and (c) Al-5 wt%NbC-1.5 wt%B_4C composites.

were quantified using the universal testing machine based on the ASTM E9–89a standard. Fig. 9a displays the engineering stress-strain curves under compressive loading on the Al-NbC-B_4C composites. It is observed that the engineering stress-strain curves have shifted to higher UCS reaching 328 MPa and a low engineering failure strain of 0.64 for Al-5 wt%NbC-2.0 wt%B_4C composite. Whereas, the pure Al has the lowest UCS of 296 MPa and undergoes the highest strain to fracture reaching 0.74. This reflects the work-hardening capability of the Al hybrid composite reinforced with NbC-B_4C ceramic particles to highly resist and withstand the applied compressive loads and significantly diminish the fracture strain (elongation). The bimodal-reinforced Al-5 wt%NbC-2.0 wt%B_4C composite has exhibited a higher UCS of 328 MPa compared to 251 MPa and 312 MPa for the Al-1.0 wt%Cu and Al-5 wt% Si_3N_4-1.5 wt%GNPs composites, respectively, which were prepared via a similar route [11,40]. Additionally, the dislocation mismatch might be induced during the compression due to the wide variations between the intrinsic strengths of ceramic reinforcements and the Al matrix. The mismatch dislocations could further inhibit the movements of other generated dislocations and then increase the work-hardening effect [44].

The slope of the engineering stress-strain is equivalent to Young's modulus, which becomes steeper with incrementing the composition of

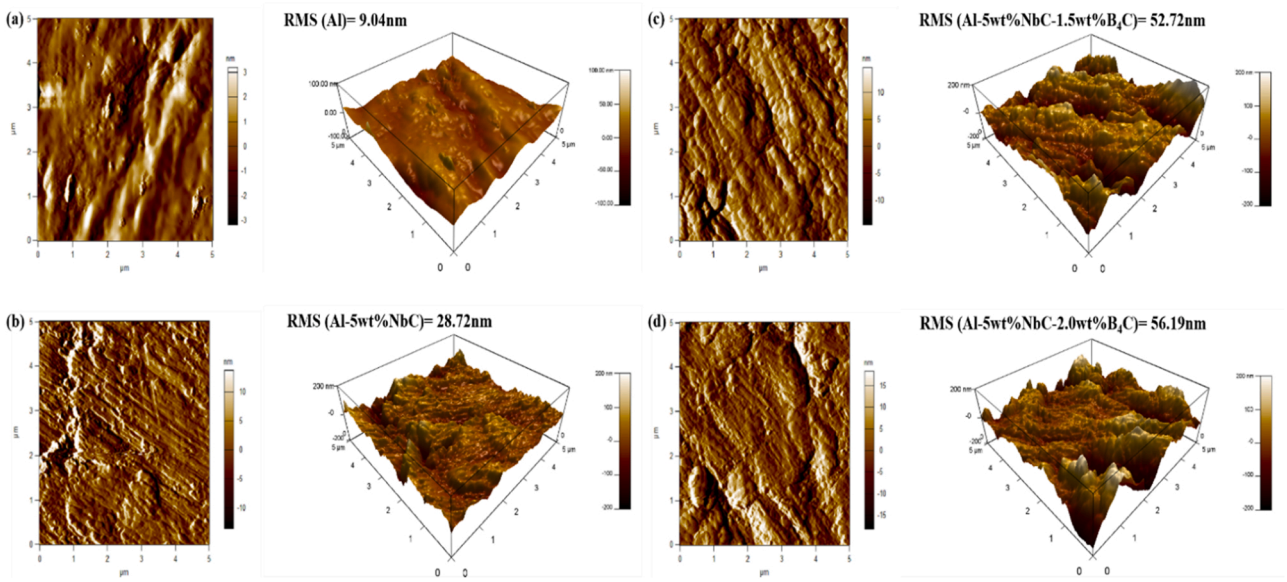

Fig. 5. 2D and 3D AFM surface images and surface roughness-mean-square (RMS) values of (a) pure Al, (b) Al-5 wt%NbC, (c) Al-5 wt%NbC-1.5 wt%B_4C, and (d) Al-5 wt%NbC-2.0 wt%B_4C composites.

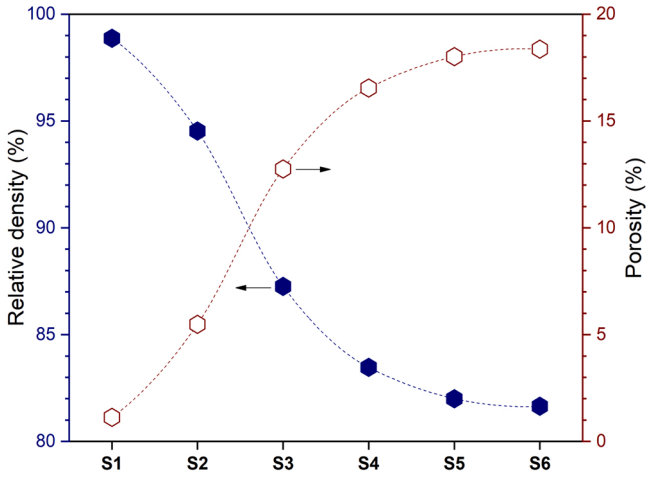

Fig. 6. Density and porosity measurements of Al-NbC-B_4C hybrid composites.

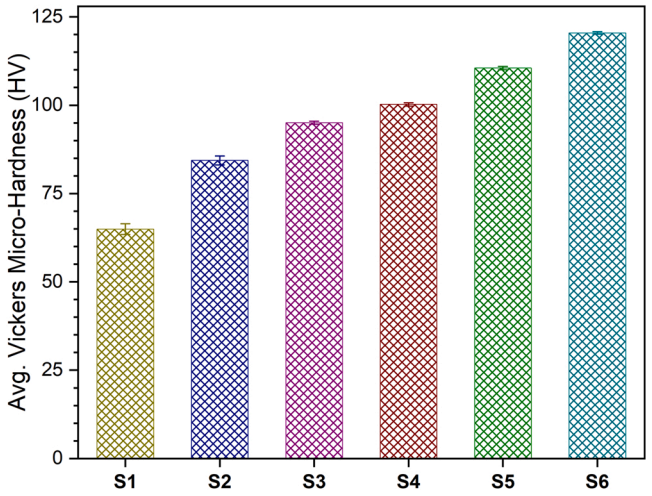

Fig. 7. Average Vickers microhardness of Al-NbC-B_4C hybrid composites.

B_4C nano-reinforcement. This points to the resistance enhancements in the Al-NbC-B_4C composites to elastic deformations and then turning into stiff and inelastic material. The Al-5 wt%NbC-2.0 wt%B_4C composite has reached a high Young's modulus of 590 MPa compared to 450 MPa for pure Al with 31% of enhancement. The mono-modal composite reinforced with micro-sized NbC particles shows Young's modulus of 570 MPa with 21% of enhancements over pure Al. This point to the nonsubstantial grain refinement and load transfer with only micro-sized reinforcement strengthening. The Young's modulus value of 590 MPa for Al-5 wt%NbC-2.0 wt%B_4C composite overcomes the 139 MPa for Al-5 wt%SiC-9.0 wt%TiO_2 hybrid composite prepared by a similar route [10] and 325 MPa for Al-20 wt%B_4C mono-modal composite synthesized via milling followed by microwave sintering and hot extrusion [39]. Alternatively, the mismatch in the coefficient of thermal expansion (CTE) between NbC micro-reinforcement (6.5×10^{-6} K^{-1}) and Al matrix (26×10^{-6} K^{-1}) particles is likely to promote the dispersion strengthening mechanism within Al composites [45,46]. Therefore, hindering the dislocation movement in the Al matrix and then increasing the composite strength. In literature, the bimodal-sized hybrid composites showed improved strength owed to nano-reinforcement, while improved ductility owed to micro-reinforcement [6]. Thus, increasing the amount of B_4C while maintaining the NbC composition fixed leads to improvement in the UCS and Young's modulus through synergistic load transfer and dislocation strengthening.

3.2.4. *FE-SEM fractography analysis of Al-NbC-B_4C hybrid composites*

The FE-SEM was also used to conduct the fractography analysis on the composite pellets before and after undergoing the engineering compression test. Fig. 10 shows the improvements in the resistance mechanism to crack propagation along Al composite structures. The composite strength improvement is ascribed to the synergistic existence of 4 main strengthening mechanisms within the NbC-B_4C ceramic reinforced Al matrix composites namely the load transfer, grain refinement, Orowan looping system, and matrix-reinforcement mismatch in CTE producing dislocation strengthening [47]. The load transfer strengthening mechanism depends on the strength of the interfacial bond existing between reinforcement and matrix to transfer sufficient load from soft Al matrix to hard ceramic reinforcements. The grain refinement resulted from the reduction in composite grains size using mechanical ball milling and insignificant grains growth through rapid and homogenous microwave sintering. The Orowan looping system

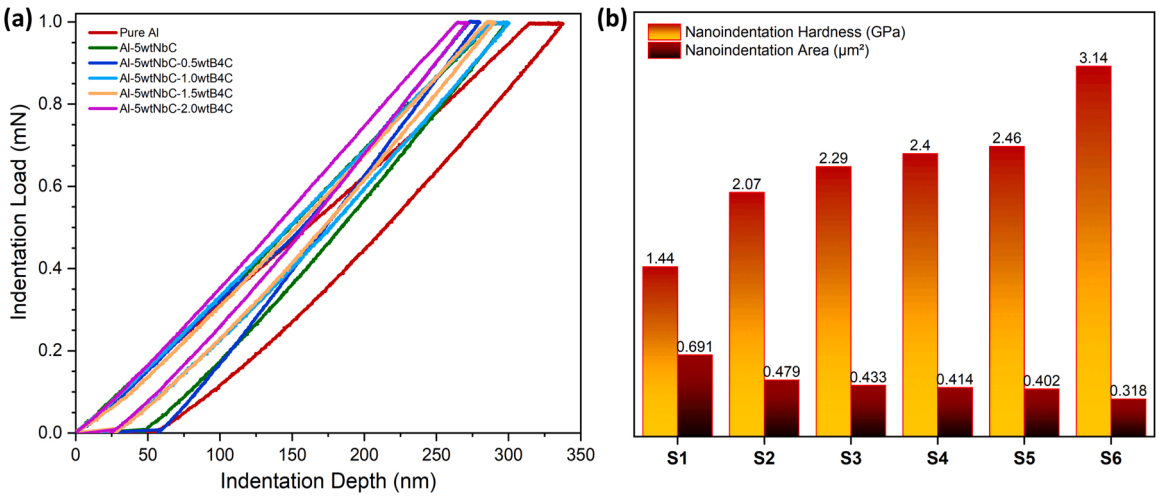

Fig. 8. Load-indentation depth curves (a) and nanohardness measurements (b) of the Al-NbC-B_4C composites.

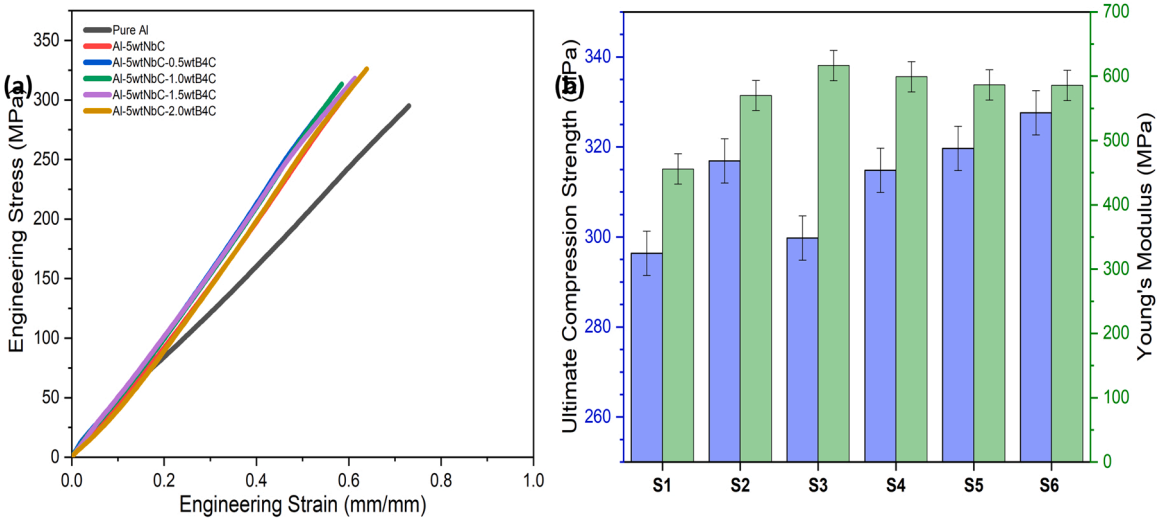

Fig. 9. Engineering compression stress-strain curves (a) and compression measurements (b) on the Al-NbC-B_4C composites.

explains the inhibition of dislocation propagation by insoluble bimodal-sized reinforcement phases.

The significant CTE mismatch occurring between NbC-B_4C reinforcements and Al matrix results in the generation of dislocations during microwave sintering. The movement of the increased dislocation density across the Al matrix will strengthen the Al composites. The FE-SEM compressive fractography in Fig. 10 reveals the enhanced dispersion hardening effect from reinforcing soft Al matrix with hard ceramic particles in micro and nano-sizes to obstacle the cracks of different lengths and then strengthing the material in resisting fracture failure. Additionally, the uniformly dispersed hard reinforcement particles throughout the Al matrix could promote the nucleation of dislocation loops. The interaction of the reinforced particles and dislocations might create dislocation loops resisting further crack propagation. Fig. 10f shows the Al-5 wt%NbC-2.0 wt%B_4C composite without noticeable signs of surface cracks in response to a pre-applied compressive loading. However, the pure Al shows the surface crack initiation and propagation along an angle of 45° to the compression axis, as displayed in Fig. 10d. The FE-SEM fractography for mono-reinforced Al-5 wt%NbC composite demonstrates the existence of more shear bands. Thus, lack of debonding between NbC reinforcement and the Al matrix. This suggests the occurrence of shear mode, which is consistent with the literature results [10,11].

4. Conclusions

Al matrix composites reinforced with bimodal-sized hybrid NbC-B_4C ceramic particles were fabricated via ball milling and microwave sintering. XRD patterns and TEM micrographs showed the formation of Al-NbC-B_4C hybrid composites in high crystallinity and grain refinement microstructures. FE-SEM micrographs with corresponding elemental mapping revealed a homogenous elemental distribution of synthesized Al-NbC-B_4C composites. AFM surface topography images and incrementing RMS values from 9.04 nm for pure Al to 56.19 nm for Al-5 wt% NbC-2.0 wt%B_4C composite confirmed the formation of hybrid composite structure with insoluble dispersed phases of hard ceramic particles into the Al matrix. The Al-5 wt%NbC-2.0 wt%B_4C composite showed an ultrahigh Vickers microhardness of 120HV, nanohardness of 3.14 GPa, Young's modulus of 586 MPa, and ultimate compressive strength of 328 MPa. FE-SEM compression fractography analysis confirmed the development of crack resistance mechanisms by reinforcing Al with micro- and nano-ceramic particles to obstacle the cracks propagation and suggest the shear mode fracture. The bimodal hybrid ceramic reinforcements enhancements on the mechanical properties of Al-NbC-B_4C composites are attributed to the simultaneous occurrence of four main strengthening mechanisms namely the thermal expansion coefficient mismatch generating dislocation strengthening, Orowan

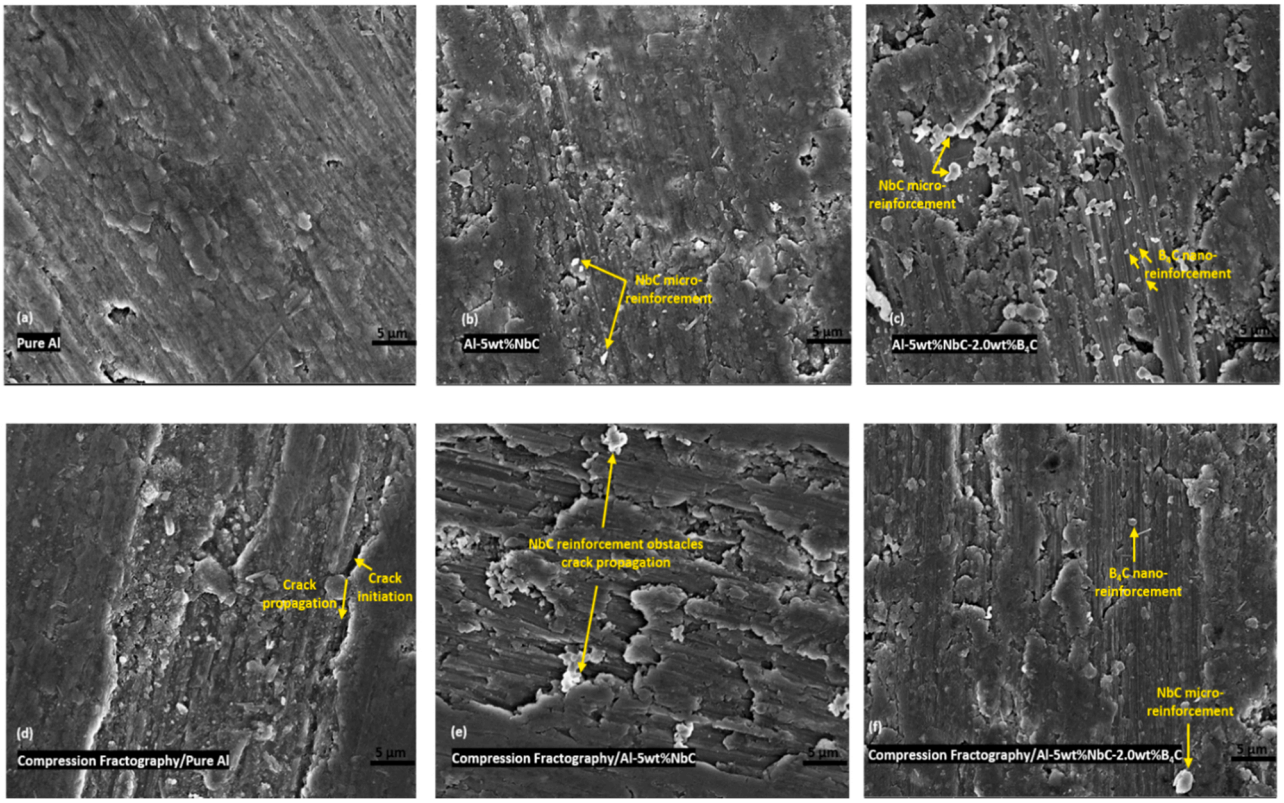

Fig. 10. FE-SEM compression fractography analysis of the Al-NbC-B_4C composites. FE-SEM images before (top row) and after (bottom row) compression test on (a,d) pure Al, (b,e) Al-5 wt%NbC, and (c,f) Al-5 wt%NbC-2.0 wt%B_4C composites.

looping system, load transfer, and grain refinement. This synergistic effect of strengthening mechanisms has been well preserved through the optimized fabrication route based on short-time mechanical milling and homogenous microwave sintering. In return, the mechanical performance of Al-5 wt%NbC-2.0 wt%B_4C composite has been enhanced remarkably over the pure Al. This reflects the strength of bimodal hybrid reinforcement for further development of Al matrix composites, particularly for applications demanding adequate resistance to crack propagation.

CRediT authorship contribution statement

Aicha S. Lemine: Methodology, Validation, Data curation, Formal analysis, Investigation, Writing - original draft. **Osama Fayyaz:** Methodology, Conceptualization, Supervision, Validation, Writing – review & editing. **Moinuddin Yusuf:** Resources, Formal analysis. **R.A. Shakoor:** Conceptualization, Supervision, Validation, Writing – review & editing, Project administration, Resources. **Zubair Ahmad:** Validation, Resources, Writing – review & editing. **Jolly Bhadra:** Writing – review & editing, Resources. **Noora J. Al-Thani:** Writing – review & editing, Resources.

Declaration of Competing Interest

The authors declare that they have no known competing financial interests or personal relationships that could have appeared to influence the work reported in this paper.

Data availability

The data that has been used is confidential.

Acknowledgments

This work was supported by Qatar University Grant no. GTRA-17722. The statements made herein are solely the responsibility of the authors. The authors would like to acknowledge the technical support from the Central Laboratory Unit (CLU) at Qatar University. Open Access funding is provided by the Qatar National Library.

References

[1] A.K. Sharma, R. Bhandari, A. Aherwar, R. Rimašauskiene, C. Pinca-Bretotean, A study of advancement in application opportunities of aluminum metal matrix composites, Mater. Today Proc. 26 (2020) 2419–2424, https://doi.org/10.1016/j.matpr.2020.02.516.

[2] T. Han, F. Wang, J. Li, N. Zhao, C. He, Simultaneously enhanced strength and ductility of Al matrix composites through the introduction of intragranular nano-sized graphene nanoplates, Compos. Part B Eng. 212 (2021), 108700, https://doi.org/10.1016/j.compositesb.2021.108700.

[3] M.O. Bodunrin, K.K. Alaneme, L.H. Chown, Aluminium matrix hybrid composites: a review of reinforcement philosophies; Mechanical, corrosion and tribological characteristics, J. Mater. Res Technol. 4 (2015) 434–445, https://doi.org/10.1016/j.jmrt.2015.05.003.

[4] B. Vijaya Ramnath, C. Elanchezhian, M. Jaivignesh, S. Rajesh, C. Parswajinan, A. Siddique Ahmed Ghias, Evaluation of mechanical properties of aluminium alloy-alumina-boron carbide metal matrix composites, Mater. Des. 58 (2014) 332–338, https://doi.org/10.1016/j.matdes.2014.01.068.

[5] X. Chen, Z. Xu, D. Fu, H. Zhang, J. Teng, F. Jiang, Comparative hot workability characteristics of an Al–Si/SiCp aluminium matrix composite hybrid reinforced with various TiB2 additions, Metals Mater. Int. 27 (2021) 1880–1891, https://doi.org/10.1007/s12540-019-00585-9.

[6] P. Nyanor, O. El-Kady, H.M. Yehia, A.S. Hamada, M.A. Hassan, Effect of bimodal-sized hybrid TiC–CNT reinforcement on the mechanical properties and coefficient of thermal expansion of aluminium matrix composites, Metals Mater. Int. 27 (2021) 753–766, https://doi.org/10.1007/s12540-020-00802-w.

[7] B. Sadeghi, M. Shamanian, F. Ashrafizadeh, P. Cavaliere, M. Sanayei, J.A. Szpunar, Microstructural behaviour of spark plasma sintered composites containing bimodal micro- and nano-sized Al2O3 particles, Powder Metall. 61 (2018) 50–63, https://doi.org/10.1080/00325899.2017.1391504.

[8] M.C. Şenel, Y. Kanca, M. Gürbüz, Reciprocating sliding wear properties of sintered Al-B4C composites, Int J. Min. Metall. Mater. 24 (2022) 584–593, https://doi.org/10.1007/s12613-020-2243-5.
[9] C. Yuan, Z. Tan, G. Fan, M. Chen, Q. Zheng, Z. Li, Fabrication and mechanical properties of CNT/Al composites via shift-speed ball milling and hot-rolling, J. Mater. Res. 34 (2019) 2609–2619, https://doi.org/10.1557/jmr.2019.219.
[10] M.R. Mattli, P.R. Matli, A. Khan, R.H. Abdelatty, M. Yusuf, A. Al Ashraf, et al., Study of microstructural and mechanical properties of al/sic/tio2 hybrid nanocomposites developed by microwave sintering, Crystals (2021) 11, https://doi.org/10.3390/cryst11091078.
[11] R. Abdelatty, A. Khan, M. Yusuf, A. Alashraf, R.A. Shakoor, Effect of silicon nitride and graphene nanoplatelets on the properties of aluminum metal matrix composites, Materials (2021) 14, https://doi.org/10.3390/ma14081898.
[12] A. Khan, M.W. Abdelrazeq, M.R. Mattli, M.M. Yusuf, A. Alashraf, P.R. Matli, R. A. Shakoor, Structural and mechanical properties of Al-SiC-ZrO2 nanocomposites fabricated by microwave sintering technique, Crystals 10 (10) (2020) 904, https://doi.org/10.3390/cryst10100904.
[13] Sumankant Yashpal, C.S. Jawalkar, A.S. Verma, N.M. Suri, Fabrication of aluminium metal matrix composites with particulate reinforcement: a review, Mater. Today Proc. 4 (2017) 2927–2936, https://doi.org/10.1016/j.matpr.2017.02.174.
[14] H. Ghandvar, M.A. Jabbar, S.S. Rahimian Koloor, M. Petru, A. Bahador, T.A. Abu Bakar, et al., Role b4c addition on microstructure, mechanical, and wear characteristics of al-20%mg2si hybrid metal matrix composite, Appl. Sci. 11 (2021) 1–22, https://doi.org/10.3390/app11073047.
[15] B. Hekner, J. Myalski, P. Wrześniowski, T. Maciąg, Al matrix composites reinforced by Ti and C dedicated to work at elevated temperature, Materials (2021) 14, https://doi.org/10.3390/ma14113114.
[16] O. Carvalho, M. Buciumeanu, S. Madeira, D. Soares, F.S. Silva, G. Miranda, Mechanisms governing the mechanical behavior of an AlSi-CNTs-SiCp hybrid composite, Compos. Part B Eng. 90 (2016) 443–449, https://doi.org/10.1016/j.compositesb.2016.01.032.
[17] A. Tan, J. Teng, X. Zeng, D. Fu, H. Zhang, Fabrication of aluminium matrix hybrid composites reinforced with SiC microparticles and TiB2 nanoparticles by powder metallurgy, Powder Metall. 60 (2017) 66–72, https://doi.org/10.1080/00325899.2016.1274816.
[18] A. Chaubey, P. Konda Gokuldoss, Z. Wang, S. Scudino, N. Mukhopadhyay, J. Eckert, Effect of particle size on microstructure and mechanical properties of al-based composite reinforced with 10 vol% mechanically alloyed Mg-7.4%al particles, Technologies 4 (2016) 37, https://doi.org/10.3390/technologies4040037.
[19] D.N. Travessa, M.J. Silva, K.R. Cardoso, Niobium carbide-reinforced Al matrix composites produced by high-energy ball milling, Metall. Mater. Trans. B Process Metall. Mater. Process Sci. 48 (2017) 1754–1762, https://doi.org/10.1007/s11663-017-0959-z.
[20] M.V.M. Souto, C.P.B. De Araujo, M.J.S. Lima, F.M.M. Borges, U.U. Gomes, C.P. De Souza, Synthesis and characterization of niobium carbide with copper addition obtained via gas solid reaction, Mater. Res. (2018) 21, https://doi.org/10.1590/1980-5373-MR-2016-1108.
[21] J. Ding, C. Cui, Y. Sun, L. Kang, L. Zhao, Interfacial characterization and high-temperature property of NbB2+NbC nanoparticles-reinforced 2219Al matrix composite synthesized by melt spinning, Adv. Eng. Mater. 22 (2020) 1–8, https://doi.org/10.1002/adem.202000248.
[22] D.K. Sharma, M. Sharma, G. Upadhyay, Boron carbide (B4C) reinforced aluminum matrix composites (AMCs), Int. J. Innov. Technol. Explor Eng. 9 (2019) 2194–2203, https://doi.org/10.35940/ijitee.A4766.119119.
[23] R. Harichandran, N. Selvakumar, Effect of nano/micro B4C particles on the mechanical properties of aluminium metal matrix composites fabricated by ultrasonic cavitation-assisted solidification process, Arch. Civ. Mech. Eng. 16 (2016) 147–158, https://doi.org/10.1016/j.acme.2015.07.001.
[24] S. Polat, Y. Sun, E. Çevík, H. Colijn, Microstructure and synergistic reinforcing activity of GNPs-B4C dual-micro and nano supplements in Al-Si matrix composites, J. Alloy. Compd. 806 (2019) 1230–1241, https://doi.org/10.1016/j.jallcom.2019.06.342.
[25] Wang P., Eckert J., Prashanth K Gokuldoss, Wu M Wei, Kaban I., Xi L Xia, et al. A review of particulate-reinforced aluminum matrix composites fabricated by selective laser melting. vol. 30. 2020. https://doi.org/10.1016/S1003–6326(20)65357–2.
[26] G. Manohar, A. Dey, K.M. Pandey, S.R. Maity, Fabrication of metal matrix composites by powder metallurgy: a review, AIP Conf. Proc. 1952 (2018), https://doi.org/10.1063/1.5032003.
[27] V. Soleimanian, M. Mojtahedi, A comparison between different X-ray diffraction line broadening analysis methods for nanocrystalline ball-milled FCC powders, Appl. Phys. A Mater. Sci. Process 119 (2015) 977–987, https://doi.org/10.1007/s00339-015-9054-y.
[28] M.T. Marques, A.M. Ferraria, J.B. Correia, A.M.B. Rego, R. do, Vilar, X.P.S. XRD, and SEM characterisation of Cu-NbC nanocomposite produced by mechanical alloying, Mater. Chem. Phys. 109 (2008) 174–180, https://doi.org/10.1016/j.matchemphys.2007.10.032.
[29] Z. Xu, C. Li, X. Liu, J. Yi, H. Guan, N. Li, In situ Al 4C 3 nanorods and carbon nanotubes hybrid-reinforced aluminum matrix composites prepared by a novel two-step ball milling, J. Mater. Res. 34 (2019) 1248–1257, https://doi.org/10.1557/jmr.2018.462.
[30] H. Kwon, M. Estili, K. Takagi, T. Miyazaki, A. Kawasaki, Combination of hot extrusion and spark plasma sintering for producing carbon nanotube reinforced aluminum matrix composites, Carbon 47 (2009) 570–577, https://doi.org/10.1016/j.carbon.2008.10.041.
[31] A. Pasha, B.M. Rajaprakash, Fabrication and mechanical properties of functionally graded materials: a review, Mater. Today Proc. 52 (2022) 379–387, https://doi.org/10.1016/j.matpr.2021.09.066.
[32] A.S. Lemine, F.M. El-Makaty, H.A. Al-Ghanim, K.M. Youssef, Experimental and modeling analysis of p-type Bi0.4Sb1.6Te3 and graphene nanocomposites, J. Mater. Res. Technol. 16 (2022) 1702–1712, https://doi.org/10.1016/j.jmrt.2021.12.096.
[33] C.L. Li, Q.S. Mei, J.Y. Li, F. Chen, Y. Ma, X.M. Mei, Hall-Petch relations and strengthening of Al-ZnO composites in view of grain size relative to interparticle spacing, Scr. Mater. 153 (2018) 27–30, https://doi.org/10.1016/j.scriptamat.2018.04.042.
[34] S.N. Naik, S.M. Walley, The Hall–Petch and inverse Hall–Petch relations and the hardness of nanocrystalline metals, J. Mater. Sci. 55 (2020) 2661–2681, https://doi.org/10.1007/s10853-019-04160-w.
[35] E. Novitskaya, K. Karandikar, K. Cummings, M. Mecartney, O.A. Graeve, Hall-Petch effect in binary and ternary alumina / zirconia / spinel composites, J. Mater. Res Technol. 11 (2021) 823–832, https://doi.org/10.1016/j.jmrt.2021.01.058.
[36] J. Huebner, D. Kata, P. Rutkowski, P. Petrzak, J. Kusiński, Grain-boundary interaction between Inconel 625 and WC during laser metal deposition, Materials (2018) 11, https://doi.org/10.3390/ma11101797.
[37] M. Penchal Reddy, R.A. Shakoor, A.M.A. Mohamed, M. Gupta, Microwave rapid sintering of al-metal matrix composites: a review on the effect of reinforcements, microstructure and mechanical properties, Metals (2016) 6, https://doi.org/10.3390/met6070143.
[38] P. Palmero, Structural ceramic nanocomposites: a review of properties and powders' synthesis methods, Nanomaterials 5 (2015) 656–696, https://doi.org/10.3390/nano5020656.
[39] E. Ghasali, M. Alizadeh, T. Ebadzadeh, A.H. Pakseresht, A. Rahbari, Investigation on microstructural and mechanical properties of B4C-aluminum matrix composites prepared by microwave sintering, J. Mater. Res Technol. 4 (2015) 411–415, https://doi.org/10.1016/j.jmrt.2015.02.005.
[40] S. Nawathe, W.L.E. Wong, M. Gupta, Using microwaves to synthesize pure aluminum and metastable Al/Cu nanocomposites with superior properties, J. Mater. Process Technol. 209 (2009) 4890–4895, https://doi.org/10.1016/j.jmatprotec.2009.01.009.
[41] B. Xiong, K. Liu, W. Xiong, X. Wu, J. Sun, Strengthening effect induced by interfacial reaction in graphene nanoplatelets reinforced aluminum matrix composites, J. Alloy. Compd. 845 (2020), 156282, https://doi.org/10.1016/j.jallcom.2020.156282.
[42] J. Leng, Y. Dong, B. Ren, R. Wang, X. Teng, Effects of graphene nanoplates on the mechanical behavior and strengthening mechanism of 7075al alloy, Materials 13 (2020) 1–13, https://doi.org/10.3390/ma13245808.
[43] A. Sharma, V.M. Sharma, B. Sahoo, J. Joseph, J. Paul, Study of nano-mechanical, electrochemical and raman spectroscopic behavior of al6061-sic-graphite hybrid surface composite fabricated through friction stir processing, J. Compos. Sci. (2018) 2, https://doi.org/10.3390/jcs2020032.
[44] Z.Y. Liu, B.L. Xiao, W.G. Wang, Z.Y. Ma, Modelling of carbon nanotube dispersion and strengthening mechanisms in Al matrix composites prepared by high energy ball milling-powder metallurgy method, Compos. Part A Appl. Sci. Manuf. 94 (2017) 189–198, https://doi.org/10.1016/j.compositesa.2016.11.029.
[45] T.H. Nam, G. Requena, P. Degischer, Thermal expansion behaviour of aluminum matrix composites with densely packed SiC particles, Compos. Part A Appl. Sci. Manuf. 39 (2008) 856–865, https://doi.org/10.1016/j.compositesa.2008.01.011.
[46] C.P. Kempter, E.K. Storms, Thermal expansion of some niobium carbides, J. Less-Common Met 13 (1967) 443–447, https://doi.org/10.1016/0022-5088(67)90037-9.
[47] S. Chand, P. Chandrasekhar, R.K. Sarangi, R.K. Nayak, Influence of B4C particles on processing and strengthening mechanisms in aluminum metal matrix composites -A review, Mater. Today Proc. 18 (2019) 5356–5363, https://doi.org/10.1016/j.matpr.2019.07.562.